UC Berkeley
UC Berkeley Previously Published Works

Title

Performance implications of chemical mobilization after microchannel IEF

Permalink

Journal

ISSN

Authors

Tentori, Augusto M
Herr, Amy E

Publication Date

DOI

Peer reviewed

Yuchen Pan
Kelly Karns
Amy E. Herr

Graduate Program in
Bioengineering, University of
California San Francisco and
University of California Berkeley,
CA, USA

Review

Microfluidic electrophoretic mobility shift assays for quantitative biochemical analysis

Electrophoretic mobility shift assays (EMSAs) play an important role in analytical chemistry, quantitative bioscience, and point-of-care diagnostics. Emerging microfluidic lab-on-a-chip technologies bring high throughput and multiplexed analysis to affinity-based electrophoretic separations, greatly advancing the performance of traditional EMSAs. This review elaborates on the relevant theoretical basis for EMSAs, surveys microfluidic-based EMSA applications in molecular conformation analyses, immunoassays, affinity assays and genomics, and outlines challenges and potential future improvements needed from this powerful assay.

1 Mobility shift assays are ubiquitous in bioanalysis

The past few decades have seen tremendous development of microfluidic electrophoresis tools [1]. These tools are becoming a powerful paradigm for quantitative and robust bioanalytical separations; in turn, advancing the fields of proteomics [2] and genomics [3]. Like its conventional macroscale counterpart, microfluidic electrophoresis separates biomolecules based on differences in the electrophoretic mobilities of the species. Electrophoretic mobility shift assays (EMSAs), sometimes referred to as gel retardation assays, are one class of affinity-based electrophoresis assays that utilize a molecular probe to impart size and/or charge change to the analytes, thus inducing an electrophoretic mobility shift. The resultant shift enables electrophoretic separation of the different molecular populations. Owing to favorable scaling with miniaturization, enhanced heat dissipation allows use of much higher electric fields than conventional macroscale formats, bringing faster separations and greater resolving power. Consequently, microfluidic EMSAs are ideal platforms for analyzing minute differences in biomolecular mobility.

Sophisticated microfluidic mobility shift assays have been proposed and designed that enable quantitative measurement of different classes of biomolecules. Historically speaking, EMSAs are affinity electrophoresis used to study protein–DNA or protein–RNA interactions; however, gel shift assays need not be limited to the study of protein–nucleic acid interactions. Protein–peptides [4] and protein–protein [5] interactions have also been studied with the same electrokinetic principle. Herein we intend the term EMSAs to refer to all analytical assays that rely on induced mobility shifts to render different populations of species detectable by electrophoretic separations. In this review, we will elaborate on current efforts that implement quantitative EMSAs on microfluidic formats. These assays open the door to a myriad of biomedical applications including drug screening [6], RNA conformational analysis [7], proximal fluid diagnostics [8], and enantiomer selection [9]. Other affinity-based EMSAs have been comprehensively reviewed elsewhere [10–13], in terms of CE [10,11], clinical relevance [12], and drug discovery [13].

Electrophoretic mobility is an intrinsic physical property of a biomolecule and is related to biomolecular size, charge, and the viscosity of the separation medium. Equation (1) represents the relationship between these quantitative variables:

$$\mu_{EP} = \frac{z \cdot e}{6\pi a \upsilon}. \tag{1}$$

where μ_{EP} is the electrophoretic mobility, z is the biomolecular charge, a is the hydrodynamic radius of the biomolecule, and υ is the viscosity of the separation medium. In EMSAs, molecular interactions alter the charge-to-radius ratio (z/a) of molecules that induces a mobility shift detectable during electrophoretic separation. Figure 1 schematically illustrates primary sources of affinity-based electrophoretic mobility shifts.

Three main classes of EMSAs will be covered. First, we discuss EMSAs that utilize a small molecular probe (target) to induce a detectable change in molecular conformation. These assays shed light on the thermodynamic process of

Correspondence: Dr. Amy E. Herr, Bioengineering, University of California Berkeley, 308B Stanley Hall, Berkeley, CA 94720, USA
E-mail: aeh@berkeley.edu
Fax: +1-510-642-5835

Abbreviations: **AFP**, α-fetoprotein; **CL**, chemiluminescence; **EMSA**, electrophoretic mobility shift assay; **LLOD**, lower limit of detection; **PAG**, polyacrylamide gel; **PLE**, pore limit electrophoresis; **SWNT**, single-wall carbon nanotube; **TNT**, 2,4,6-trinitrotoluene

Colour Online: See the article online to view Figs. 1 and 3–5 in colour.

Mobility shift due to:
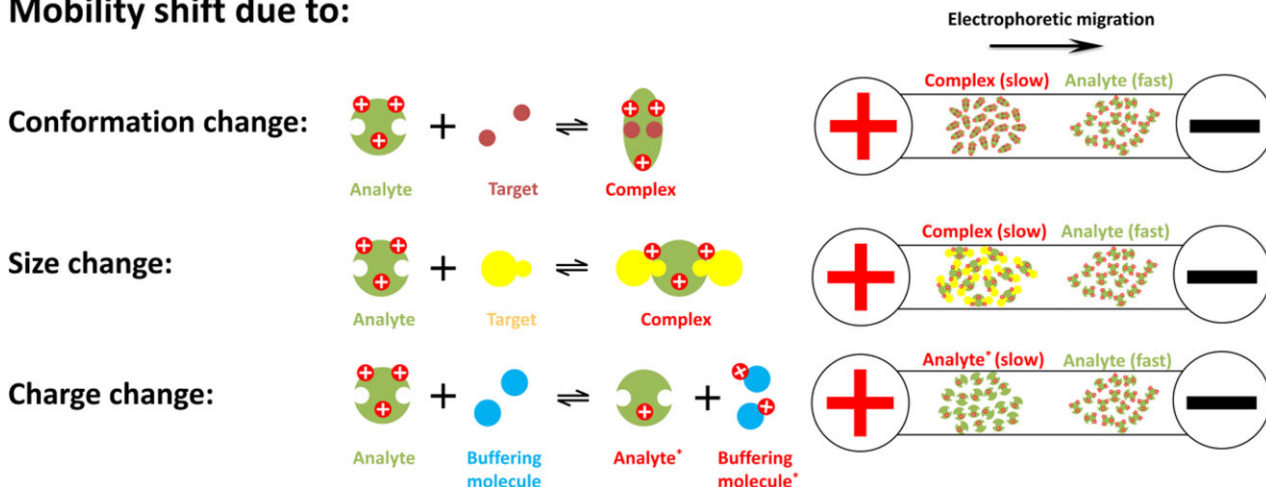
Figure 1. Conceptual schematic of EMSA principle. EMSAs can arise from conformation change: Conformation of target analyte molecule changes upon complexing with probe. The resulting molecule has a different shape than the original one, yielding a shift in mobility. EMSA due to size change: Analyte interacts with the target molecule to form a complex. The complex has a mobility that is distinct from the free form owing to a larger molecular mass. EMSA due to charge change: A buffering molecule alters the charge on an analyte, inducing a change in electrophoretic mobility of the analyte.

structural transformation. Second, we overview EMSAs that utilize an affinity probe (e.g. antibody) to induce a detectable change in the size and/or charge of a target analyte. These assays provide quantitative information on the target concentration, the binding affinity (K_d), and the kinetic rate constants (k_{on} and k_{off}) of the interactions. Third, we cover other affinity-based microfluidic EMSAs with diverse applications including DNA sizing, point mutation detection, and chiral selection. We conclude with discussion of critical challenges and potential future trends.

2 Microfluidic EMSAs are quantitative

One class of EMSAs utilizes an affinity probe that binds with a target molecule in order to induce a detectable change in electrophoretic mobility. This approach enables quantitative assessment of the concentration of the target molecule and, given proper experimental design, can also allow measurement of the equilibrium dissociation constant (K_d) of the binding pair. The K_d of two molecules provides insight into the affinity by which they bind and can be useful for understanding the affinity of drug–target interactions, among other applications. EMSA design typically allows measurement of both the molecular concentration (represented by the band signal intensity) and the mobility of migrating species (which indirectly indicates concentration). Due to the kinetic nature of the binding reaction, the bound analyte can either co-migrate with the free analyte band or resolve as a separate band. For binding pairs with a slow interconverting rate as compared to the electrophoresis timescale, free and bound analytes can be resolved during electrophoresis. In this case, concentrations of each species can be measured directly. For those pairs with binding reactions that are much faster than the electromigration timescale, the electrophoretic mobility

can be determined, from which the concentration of each analyte form (free or bound) is derived, as described in detail below:

$$\mu_{EP} = f\mu_b + (1 - f)\mu_f, \tag{2}$$

where μ_{EP}, μ_b, and μ_f are the electrophoretic mobilities of the band, bound analyte, and free analytes, respectively. f represents the fraction of bound analyte and is calculated to inform the concentration of each molecular population. For microfluidic EMSAs, the concentration is proportional to the signal intensity of the band (e.g. fluorescence, radiation) detected by the imaging system. Quantitative mobility values can be calculated by monitoring the fluorescence intensity of separating bands during the course of the electrophoretic separation. Concentration and mobility characterize the binding reaction, including the equilibrium disassociation constant K_d and kinetic rates (k_{on} and k_{off}).

2.1 Microfluidic EMSAs to measure K_d

The preceding section discusses the approaches to assess the concentrations of a binding pair. Once these values are derived from EMSAs, measurement of the equilibrium dissociation constant, K_d, can be accomplished. To calculate K_d, we first express a binding reaction involving analyte A, target analyte B, and complex AB as:

$$[A] + [B] = [AB]. \tag{3}$$

The equilibrium dissociation constant (K_d) can be written as:

$$K_d = \frac{[A] \cdot [B]}{[AB]}, \tag{4}$$

where [A], [B], and [AB] represent the concentration of free analyte, free target analyte, and bound analytes, respectively. To measure the concentration of the target analyte, a calibration curve relating initial concentration of A and the band intensity value of [AB] is helpful. For binding affinity measurement, the concentration ratio, r, between bound analyte and total analyte is:

$$r = \frac{[AB]}{[A] + [AB]} = \frac{[B]}{K_d + [B]}, \tag{5}$$

where r is expressed in concentration of each component. To transform the relationship in Eq. (5) into an expression that is relevant to any measurable, dependent system variable (e.g. immune complex concentration [AB]), we rewrite r as follows:

$$r = \frac{[AB]}{[AB]_s} = \frac{[B]}{K_d + [B]}, \tag{6}$$

where $[AB]_s$ represents the original concentration of [A] (saturated concentration of the complex).

Rearranging, we arrive at Eq. (7), known as the Scatchard equation:

$$\frac{[AB]}{[B]} = \frac{-[AB] + [AB]_s}{K_d}. \tag{7}$$

In a K_d measurement, setting [A] much lower than K_d makes changes in [B] negligible. K_d is quantified by linearly fitting [AB] and [B] to the Scatchard equation [14, 15].

In practice, analyte band intensity is proportional to the absolute analyte concentration through a coefficient k, thus obviating the need to convert the signal into a concentration. The Scatchard equation describes the equilibrium state of the binding reaction. Specifically, thermodynamic inquiry of the reaction is possible when the reaction is driven to equilibrium, meaning all concentrations have reached steady state. However, depending on the binding kinetics of the reaction, one should understand the relationship between the electromigration and reaction rates. Since $K_d = k_{off}/k_{on}$, it is possible to have the same K_d with different k_{on} and k_{off} rate constants, corresponding to different kinetic regimes. When measuring K_d, the kinetic regime in which the binding reaction resides plays an important role. In the next section, we categorize the binding reactions in terms of Damköhler number, a nondimensional number describing the scaling relationship between the reaction and migration rates. We provide a survey of microfluidic EMSA formats for analyte pairs that interconvert at varying association and dissociation rates.

2.2 Distinct Damköhler regimes impact performance

For a given K_d, the kinetics of biomolecular interactions can vary widely. As a result, molecular binding reactions fall into three distinct categories, including EMSAs with (i) rapid binding and dissociation compared to electromigration timescales, (ii) slow dissociation compared to electromigration timescales, and (iii) slow binding and fast dissociation

compared to electromigration timescales. The different kinetic regimes determine whether concentration or mobility is used for shift-based binding analysis. To quantify these regimes, we employ two Damköhler numbers relating k_{on} and k_{off} for electrophoretic separations of bound and unbound populations as:

$$Da_{on} = \frac{k_{on} L c_L}{E \mu_f}$$
$$Da_{off} = \frac{k_{off} L}{E \mu_f} \, , \tag{8}$$

where L is the separation length, c_L is the concentration of the ligand, E is the electric field, and μ_f is the mobility of the unbound molecule. The Damköhler number compares the relative magnitude of the kinetic reaction rate (either association or dissociation) and the electromigration rate. Consequently, we can ascribe EMSA behaviors to specific transport regimes using these formulations of the Damköhler number to be: (i) rapid interconversion $Da_{on} \gg 1$ and $Da_{off} \gg 1$; (ii) negligible disassociation $Da_{off} \ll 1$, and (iii) negligible re-association $Da_{on} \ll 1$ and $Da_{off} \geq 1$. In all analyses, we assume reaction equilibrium is reached before electrophoretic analysis is initiated. Intriguingly, microfluidic EMSAs offer a tool for measurement of dynamic processes, including binding reaction kinetics (i.e. k_{on} and k_{off}).

3 Microfluidic EMSAs to study molecular conformation

Biomolecular conformation encodes important biochemical information and plays a significant role in determining biological function. Owing to the small molecular radius differences between conformationally distinct molecular populations, electrophoretic mobility differences are often difficult to detect using conventional free solution or macroscale electrophoretic separations. For example, riboswitches are a class of functional RNA biomolecules that undergo a secondary structure change upon binding by a small molecule probe (e.g. metabolite). Due to the insignificant size difference, riboswitch conformational changes can be difficult to resolve on conventional native slab gel electrophoresis systems [7]. In contrast, the high electric field attainable in microfluidic channels offers better resolving power than lower field macroscale counterparts. Consequently, microfluidic EMSAs have recently been reported that enable detection of small conformation-induced mobility changes [7]. Using a successful EMSA, one can quantify the concentration/mobility of the target analyte and derive the equilibrium dissociation constant of the binding pair.

Early studies revealed the physical correlation between conformation and electrophoretic mobility. In 2007, Craighead's group [16, 17] experimentally analyzed the conformation-mobility relationship of stretched DNA in nanochannels. In their experiment, DNA was electrophoretically driven from a nanoslit into a nanochannel where a

single molecule was geometrically confined and dynamically elongated beyond its equilibrium length. The conformation, length, and mobility of the molecule were dynamically recorded by two laser-induced fluorescence detectors located on the nanochannel to show that DNA mobility increased with degree of folding. The experiment correlated the number of DNA folds to effective mobility.

The discovery of conformation-dependent mobility led to the use of molecular probes to induce detectable conformational changes to study the structure–function relationship of biomolecules. Recently, Karns et al. [7] demonstrated a microfluidic conformation change-based EMSA for the analysis of riboswitch aptamers. These small RNA genetic regulators undergo a conformational change when bound to their small molecule probes, often resulting in a compaction of molecular radius. This microfluidic EMSA analyzed two categories of SAM-1 riboswitch aptamers—each operating in a different binding regime of binding and dissociation rate constants—through the detection of a binding-induced mobility shift in a microchip polyacrylamide gel (PAG) channel. The enhanced sieving power of PAG coupled with high-resolution microfluidics enabled detection of the small mobility differences between the conformationally distinct bound and unbound riboswitch populations. The shifts were not robustly detectable using a conventional slab gel format. This and other microfluidic EMSAs provide a quantitative platform for analysis of small conformation-based mobility shifts. Such tools hold great potential for applications aimed at a wide range of target molecules including DNA origami [18] and small molecular weight messenger molecules in cell signaling systems [19].

4 Quantitative microfluidic EMSAs that utilize affinity molecular probes (target) to induce a change in analyte molecule size and/or charge

Complex formation can alter the mass and/or charge of a target analyte, thereby inducing an electrophoretic mobility shift. A broad range of biomolecules have been successfully used as affinity probes. Microfluidic affinity-based EMSAs can discriminate between bound and unbound analyte, revealing quantitative information on the analyte concentration, equilibrium dissociation constant (K_d), and kinetic rate constants (k_{on} and k_{off}). In the next sections, we will detail several classes of quantitative affinity-based microfluidic EMSAs including immunoassays (IAs), affinity EMSAs, drag-tag-based EMSAs, and others.

4.1 Microfluidic quantitative electrophoretic IAs

Assays that utilize an antibody as a molecular probe are termed "immunoassays." In EMSA IAs, the immune complex (composed of antibody and target analyte) and unbound analyte are in solution phase and assayed via electrophoresis. These assays are often called homogeneous electrophoretic IAs. Owing to the large molecular mass of the antibody, the

bound complex migrates at a lower electrophoretic velocity than either the free antigen or the free antibody. Concentrations of different molecular populations can be extracted from EMSA IAs, and in some cases the equilibrium dissociation constant of the analyte pair can also be derived. In recent years, efforts have been focused on increasing analytical sensitivity and throughput.

Quantitative electrophoretic homogeneous IAs were first adapted onto microfluidic formats in the late 1990s by Harrison and co-workers [20–22]. In this pioneering work [20], the researchers used fluorescently labeled anti-BSA antibody to detect BSA in a standard double-T channel microfluidic chip. The antibody and antigen solutions were mixed off-chip prior to on-chip EMSA. During electrophoresis, the immune complex migrated slower than the free antibody and hence the two separated from each other. The abundance of each population was measured with fluorescence quantification. The use of high electric fields greatly accelerated IA throughput. In subsequent work [21], on-chip sample mixing and reaction were coupled to the IA by incorporating dilution and mixing serpentine channels onto the main separation channel from the original design. Carefully applied voltage programming allowed controlled mixing of antibody and antigen, yielding a dose–response curve [21]. The design was scaled up into a 6-plex format integrated on a single chip to advance throughput of the quantitative analysis [22].

4.1.1 Microfluidic competitive IAs

In a competitive IA, unlabeled antigen competes with labeled antigen to bind the cognate antibody. We see from Eq. (3) that a constant amount of antigen occupies the "bound" state when unbound antibody concentration reaches a constant value. If the concentration of unlabeled analyte in the reaction solution is increased, competition between unlabeled and labeled analyte lowers the levels of bound labeled analyte. Quantification of the labeled analyte at different unlabeled analyte levels yields a calibration curve from which the concentration of the target analyte is obtained.

Bromberg et al. introduced a competitive IA on a microfluidic electrophoresis format [23] and designed a 48-plex platform by distributing the microfluidic channels radially on a circular glass substrate [24] (Fig. 2A). In their work, a mixture of fixed concentration of fluorescein-labeled 2,4,6-trinitrotoluene (TNT) and anti-TNT antibody were incubated with a varying amount of unlabeled TNT, and together analyzed on-chip. Cathode, anode, and waste reservoirs were created in two concentric PDMS rings on the 96-lane radial microchannel plate. Each single separation unit resembled that of a standard cross-channel architecture. Quantitative measurements of unlabeled TNT concentration were demonstrated over a wide dynamic range of approximately 2 to 530 nM (converted from the concentration units reported by the authors). Huang et al. coupled chemiluminescence (CL) to a competitive assay [25–28]. Here, horseradish peroxidase labeled antigen and its antibody were mixed and loaded on a
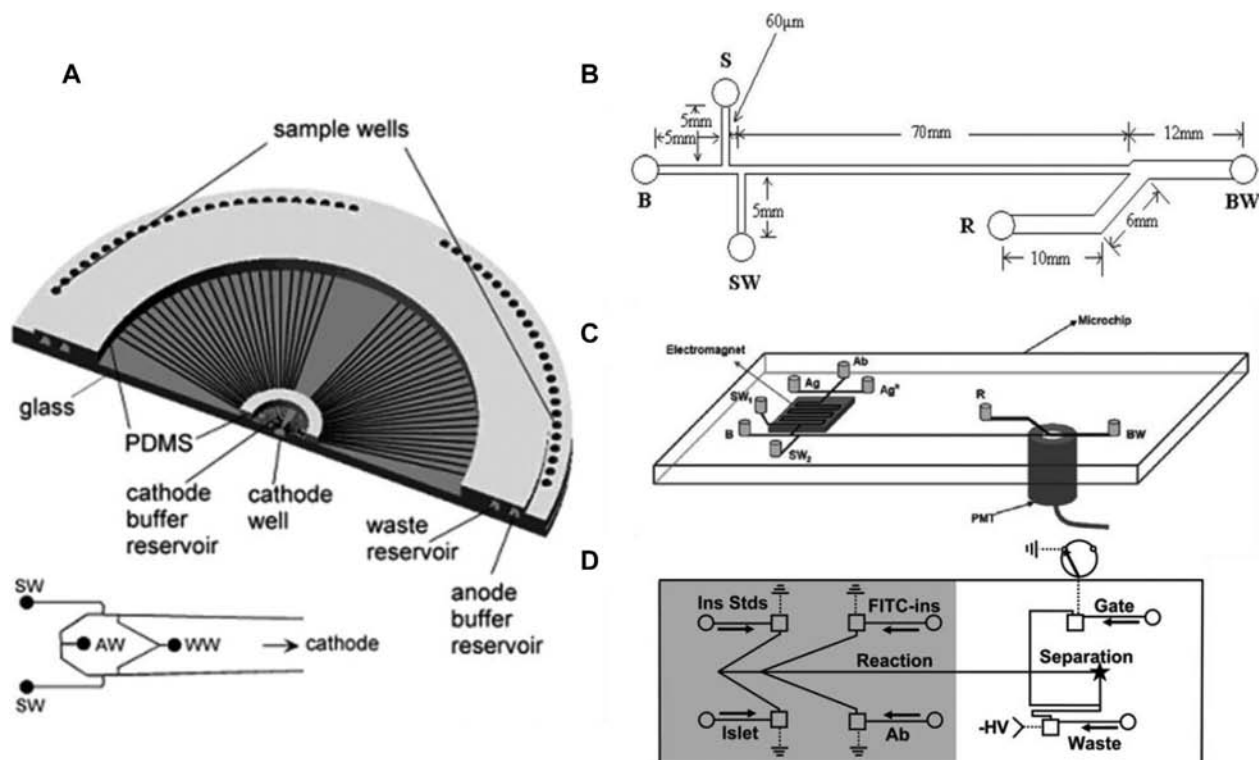
Figure 2. Microfluidic electrophoretic immunoassay configuration. (A) Schematic of the multiplexed 48-plex microchannel radially distributed around a common cathode well in the circular glass substrate. The sample wells are on the periphery and the anode and waste wells are at the center and linked to the PDMS gasket. (Reprinted from [24] with permission.) (B) Competitive immunoassay to detect T4 with chemiluminescence (CL). S: sample reservoir; B: buffer reservoir; SW: sample waste reservoir; BW: buffer waste reservoir; R: CL solution reservoir. (Reprinted from [26] with permission.) (C) Schematic of the magnetic coupled microfluidic electrophoretic immunoassay. The electromagnetic pad is placed downstream of the antibody–antigen mixing channel to immobilize the unreacted antibody. (Reprinted from [28] with permission.) (D) Device schematic of the real-time insulin measurement from islet cells. The use of relay and gate controls the flow and periodically insert a plug of analytes into the separation channel for detection. Ins Stds: insulin standards; HV: high voltage. (Reprinted from [31] with permission.)

standard double-T channel for separation. A side channel was connected downstream of the separation channel to introduce the CL reaction solution, thus allowing visualization of the analytes (Fig. 2B). Human serum proteins including testosterone [25], thyroxine [26, 29], and phenobarbital [27] were quantified. Enhanced signal was observed from enzymatic amplification and a lower LOD (LLOD) of a few nanomolar was reported.

In one modified version of the above assay, an electromagnetic pad was placed under the precolumn reactor [28]. Magnetic nanoparticle-labeled antibodies were immobilized on the floor of the reaction channel to separate bound and free analytes (Fig. 2C). This strategy yielded a straightforward separation process and may enhance the separation resolution. A multiplexed IA for five model antigens in human serum was demonstrated. Analyte concentration detection sensitivity measured via the single-plex assay was comparable to the multiplexed assay [25–27].

Microfluidic EMSAs utilizing a competitive IA format have been applied to the study of living cells. The Kennedy group [30–33] quantified the secretion levels of insulin from islet cells in real time. Their microfluidic chip (Fig. 2D) con-

sisted of four injection channels, a reaction channel, two bifurcating channels (waste/separation), and a waste reservoir. Insulin secreted by the islet cells was introduced into the reaction channel by grounding the islet reservoir. In the reaction channel, the insulin was incubated with FITC-insulin and anti-insulin, and introduced through EOF. Using a kinetics-informed design, the competitive IA completed at the end of the reaction channel. There, a relay coupled to the channels manipulated the flow through EOF so that, every few seconds, a plug of sample was injected into the reaction channel for separation and quantitative analysis. For calibration, grounding of the islet reservoir was switched to an insulin standards reservoir. Continuous injection allowed the monitoring of the islet behavior for up to 24 h with minor modifications to the system.

4.1.2 Microfluidic EMSA with clinical relevance

Microfluidic IAs have been exploited for point-of-care diagnostics [8, 29, 34–40]. Schmalzing et al. [34] used the standard cross-channel microchip as a format for competitive IAs to detect thyroxine (T4) in human sera. A fixed amount of
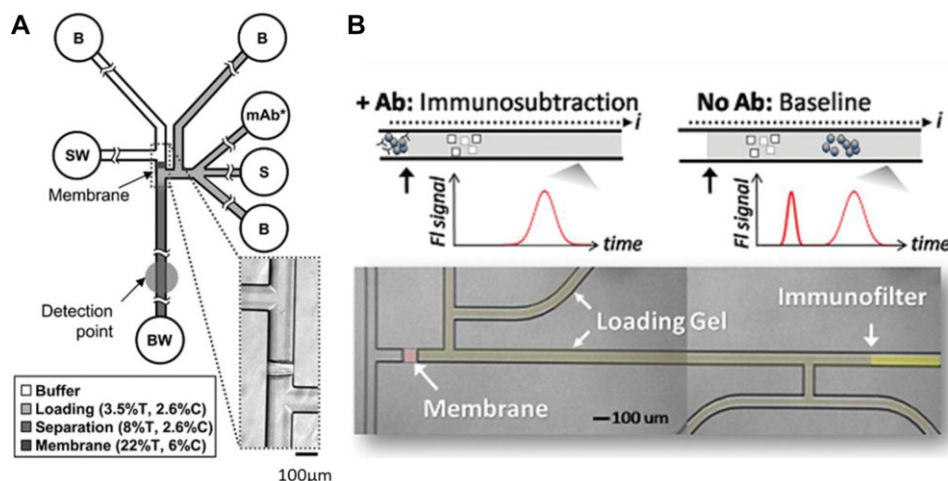
Figure 3. Microfluidic EMSA immunoassay for clinical diagnostics. (A) Microfluidic PAG assay for metalloproteinase-8 (MMP-8) analysis. A high-density PAG membrane is photopolymerized inside the channel that acts to preconcentrate the sample. The membrane is shown in the inset picture. (Reprinted from [38] with permission.) (B) Microfluidic immunosubtraction. The pink gel membrane is placed in the main separation channel to preconcentrate the analytes. The immunofilter (marked with yellow) subtracts the immunocomplex from the mixture. When antibody is present in the solution, the immunofilter excludes the specific sample peaks from the resultant PAGE electropherogram. (Reprinted from [8] with permission.)

fluorescein-labeled T4 and anti-T4 polyclonal antibody were incubated with sera and separated on-chip, from which the T4 concentration in the sera was determined. The LLOD of the assay was approximately 40 nM. The detection sensitivity was enhanced to a LLOD of 2.2 nM by introducing CL [29].

To improve the separation resolution and reduce the assay duration, PAG was used as an electrophoretic molecular sieving matrix. Herr et al. [38] developed a microfluidic point-of-care diagnostic tool for rapid saliva analysis. The assay measured the concentration of a collagen-cleaving enzyme, matrix metalloproteinase-8. In this assay, the metalloproteinase-8 and its antibody were electrophoresed against a photopatterned high-density PAG membrane in the channel, where subsequent preconcentration and reaction simultaneously occurred. The mixture was then eluted into an electrophoresis separation channel and the free antibody and complex separated from each other based on the difference in their electrophoretic mobilities (Fig. 3A). Building on this work, Apori et al. [8] introduced an immunofilter (high-density gel) inside a separation channel to establish a microfluidic immunosubtraction assay for C-reactive protein and S100B proteins in cerebrospinal fluid. Here, the antibody and antigen were introduced to the membrane and allowed to mix and bind. Subsequent elution of the mixture into the separation channel caused the antibody–antigen complex to be preferentially retained at the immunofilter (Fig. 3B). As a result, quantitative information of the binding reaction was extracted from the fluorescent signal retained by the filter (represents the concentration of the complex). Karns and Herr [39] investigated a homogeneous microfluidic electrophoretic IA for lactoferrin, a tear protein biomarker for Sjögren's syndrome. A discontinuous 3%T and 6%T PAG (%T is the total acrylamide/bisacrylamide monomer concentration by weight) was patterned inside the loading channel

and separation channel of a cross-channel microchip, respectively. The discontinuity acted to enrich the sample for better detection sensitivity. Sample analysis required less than 1 μL of human tear fluid.

In addition, Hou and Herr [40] introduced a microfluidic gradient and discontinuous PAG device for rapid homogeneous electrophoretic IAs. The gradient gel comprised a segment of PAG polymerized in the separation channel with continuously increasing acrylamide concentration and, thus, continuously decreasing gel pore size. The approach was first used to improve separation resolution in 1961 [41] with a microfluidic version introduced by Lo et al. [42] in 2008. Discontinuous PAGs were fabricated by photopatterning gel with different concentrations in the loading channel and separation channel. In the Hou and Herr work, a 2.5–5%T gradient PAG and discontinuous PAG were fabricated in the microchip. Experimental data show that a mixture of C-reactive protein and immunocomplex were fully separated within 925 μm (gradient PAG) and 319 μm (discontinuous PAG), 4 and 12 times shorter than that of a 2.5%T homogeneous PAG.

4.1.3 Microfluidic heterogeneous IAs

In heterogeneous IAs, target molecules are immobilized on a solid support or surface. Corresponding analytes are advected through the region and are captured onto the functionalized surface [43]. Upon binding to a surface-immobilized partner, the target analyte mobility shifts to zero and the resulting complex forms on the solid support. This resultant complex reveals quantitative information of the binding reaction. One demonstrated class of heterogeneous IA design utilized functionalized PAGs that were photopolymerized
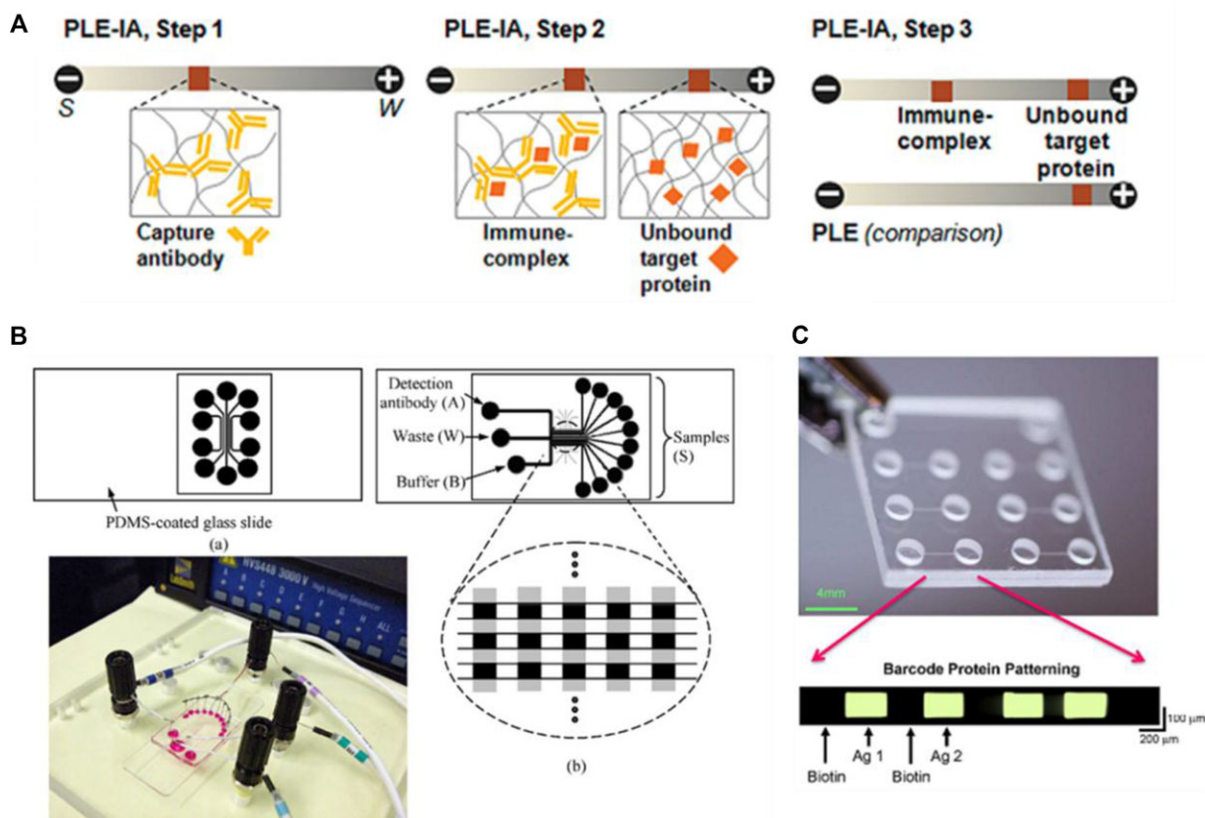
Figure 4. Heterogeneous microfluidic immunoassay. (A) Schematic showing the steps of PLE-IA. Step 1: antibody is electrophoresed in a PAG gradient gel to the pore size limit of the analyte and pseudo-immobilized. Step 2: sample containing the target protein is electrophoresed through the gradient gel. The target protein reacts with antibody and is retained. Unreacted proteins continue moving until they hit their pore limit. Step 3: comparison of PLE band patterns with and without pseudo-immobilized antibody validates the presence of the immune complex. (Reprinted from [44] with permission.) (B) Antigen barcodes are patterned on the PDMS-coated glass slide using a PDMS-gasket containing five channels in (a). A second PDMS device in (b) for the immunoassay was placed over the patterned antigen (in gray). The matrix of rectangular intersections became the reaction chambers in the assay. (Reprinted from [46] with permission.) (C) Schematic of patterned antigen capture regions along the microfluidic channel in the barcode assay, interlaced with biotin strip bands. (Reprinted from [49] with permission.)

in a microfluidic channel [44]. Target molecules were electrophoresed through the PAG and, given the correct operating conditions, were immobilized on the surface. Visualization of retained signal revealed quantitative analyte concentration. Chen et al. [44] implemented microfluidic pore limit electrophoresis (PLE) as the basis for a heterogeneous IA. Microfluidic PLE relies on a PAG with a decreasing gel pore size [45]. In PLE, the pore size is decreased to such a small size that analyte species should be "excluded" (and halt) upon reaching a PAG region with a pore size on par with molecular dimensions. Prior to the start of the assay, the PLE-IA has capture antibody immobilized at its effective pore size, which then acts to capture target antigen subsequently electrophoresed through the antibody band in the PAG. A key feature of PLE-IA is the compatibility with continuous injection of antibody, which accumulates at the pore limit, and the resulting high capture antibody concentration greatly increases the detection sensitivity. In the Chen et al. work, this approach yielded a detection limit of 0.078 nM compared to a homogeneous system limit of 5 nM. In a dual-channel sys-

tem, PLE-IA yields both the analyte molecular mass, which is based on the "pore limit" position of the analyte along a PLE gradient gel, and the analyte identity, which is based on immunodetection (Fig. 4A). The heterogeneous PLE-IA format facilitates visualization of the readout and may comprise a promising platform for the next-generation microfluidic IAs.

In addition, Gao et al. [46] developed a multiplexed microfluidic electrokinetically controlled IA and detected two specific bacterial antibodies (anti-*Escherichia coli* O157:H7 and anti-*Helicobacter pylori*) in human sera. The microfluidic device consisted of ten parallel channels sharing five perpendicular immobilized antigen bars (Fig. 4B). The matrix of rectangular intersections was used as a matrix of reaction regions. Sample solution containing antibodies was loaded in the ten sample wells and electrophoresed toward the antigens and reaction areas. A subsequent washing step removed unreacted antibody. This step was followed by introduction of fluorescently labeled secondary antibodies. Careful selection of experimental parameters (e.g. antigen immobilization

concentration, sample incubation time) was informed by numerical simulations [47, 48]. Visualization of fluorescence at the intersections reported antibody concentrations in a sample. This microfluidic ELISA variant was capable of detecting ten samples simultaneously in 22 min with a LLOD of 130 pM (*E. coli* O157:H7).

Araz et al. [49] reported a microfluidic barcode assay using a simple "single inlet, single outlet" microchannel architecture for multiplexed analyte detection. A streptavidin-functionalized PAG was fabricated in the microchannel. Biotin and biotinylated capture reagents were immobilized in discrete regions, resulting in a barcode-like pattern of capture reagents and spacers (Fig. 4C). Sample was electrophoresed through the "barcode" heterogeneous assay, allowing simultaneous detection of multiple analytes with negligible cross-reactivity. The authors optimized the barcode assay through consideration of the electromigration and binding reaction timescales. A multiplexed barcode assay for HIV and hepatitis C virus antibodies yielded a LLOD of 165 pm. Directed electromigration and reaction led to a 10 min sample incubation step and a 30 min total assay duration, an approximately tenfold reduction in duration compared to the gold-standard RIBA that requires 8–20 h for processing.

4.1.4 Other quantitative microfluidic electrophoretic IAs

In another approach, researchers combined a microfluidic electrophoresis IA with field-amplified sample stacking [50], isotachophoresis-zone electrophoresis (ITP-ZE) [51–54], and lectin electrophoresis [51]. An intrinsic enhancement in the binding reaction, accomplished by isotachophoretic focusing induced preconcentration, improved the sensitivity of the IA. Kagebayashi et al. [51] designed an on-chip affinity-based microfluidic selector for separation of two α − fetoprotein (AFP) isoforms: AFP-L1 and AFP-L3. On-line ITP mixed and enriched the AFP isoforms, DNA-conjugated antibody (DNA modification used to control the mobility of the immune complex), and fluorescent dye into a small zone. After complete stacking, ITP was terminated and switched to zone electrophoresis to separate the immune complex from the free antibody. Lectin, which has different binding affinities towards the two isoforms, was placed in the separation channel to distinguish the two isoforms and improve the separation resolution. Due to the ITP preconcentration and enhanced resolving power afforded by the lectins, the detection limit of AFP-L3 went down to 100 fg/mL (∼1.42 fM), which is the lowest ever reported on a microchip electrophoretic IA.

4.2 Microfluidic EMSA for K_d measurement

As discussed, K_d measurements in different kinetic regions require different experimental approaches. For K_d determination in EMSAs of fast interconverting binding pairs that yield one migrating peak, a weighted mobility of free and bound analytes is recorded and concentrations are calculated using Eq. (2). For K_d determination in EMSAs of slow interconverting binding pairs that yield resolvable, distinct peaks for the bound and free analyte, concentration information is directly measured from the peak area under the curve. A detailed discussion of each kinetic Damköhler regime, as related to K_d determination, follows here.

4.2.1 Rapid interconversion regime: Fast binding rate and fast dissociation rate relative to the electromigration timescale ($Da_{on} \gg 1$ and $Da_{off} \gg 1$)

In this regime, both the association and dissociation reactions occur faster than the characteristic electromigration timescale. During electrophoretic migration, any dissociation is overcome by rapid reassociation before the two analytes are electrophoretically resolved. As such, the bound and unbound analyte populations will migrate together as a single band whose mobility is the weighted average of the two individual states [55], μ_{AB} and μ_A. A slight modification to Eq. (2) yields:

$$\mu = \frac{[AB]\,\mu_{AB} + [A]\,\mu_A}{[A] + [AB]}. \tag{9}$$

Equation (9) is used to calculate the concentrations of bound and unbound analytes, A and AB, respectively, by knowing the apparent mobility of the single band. In the rapid interconversion regime, the assumption is made that the separation will not change the local concentration of the analytes during migration.

Various groups have demonstrated microfluidic EMSAs that measure K_d for rapidly interconverting binding pairs. Chuang et al. [56] fabricated a PEG-modified cross-channel glass microchip, which was free of surface charge adsorption, to measure K_d of estrogen receptor and estrogen response elements. The binding disassociation constant K_d was measured via the mobilities of the fluorescently labeled estrogen response element. Using the same assay, the authors tested the influence of several agonists and antagonists on the binding reaction.

In other cases, the analyte is introduced into the run buffer to provide a constant background concentration for the affinity reaction, thus helping to ensure the integrity of the migrating band. In this way, Stettler et al. [57] measured the K_d of two neurotransmitters, epinephrine and norepinephrine, and their target receptor molecule, sulfated-cyclodextrin, on the Shimadzu MCE-2010 microchip. The mobilities, and then concentration of neurotransmitters were measured by UV detection with DMSO as an internal standard. From these data, K_d was derived. The same methods [58] were later used to quantitatively determine the K_d between acid-rich diketopiperazine receptors and basic tripeptides in aqueous solution. The measured K_d matched isothermal titration calorimetry results.
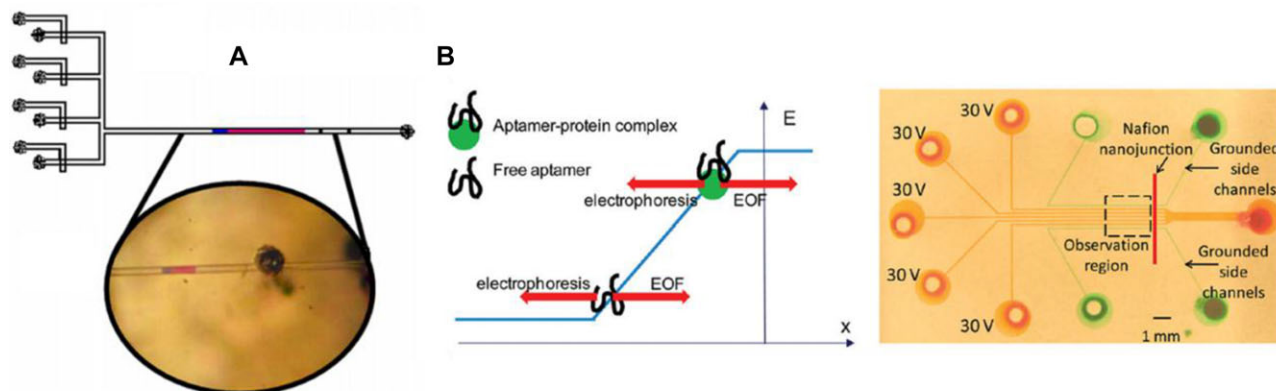
Figure 5. Microfluidic electrophoretic affinity assay. (A) Schematic of partially filled affinity microfluidic CE. The ligand (indicated by red dye) followed by the substrate (indicated by blue dye) is pressure driven into the microchannel. A capillary is connected to the end of the microchannel in which the binding reaction takes place. (Reprinted from [59] with permission.) (B) Schematic of electrokinetic concentration affinity probe electrophoresis assay. The Nafion membrane is used to generate a concentration polarization effect that forms a high electric field in the vicinity. (Reprinted from [65] with permission.)

Brown et al. [59] designed a partially filled ACE device to study the interaction between carbonic anhydrase and aryl-sulfonamide. In this work, a long plug of target molecule was injected into the microchannel using pressure followed by injection of a second short analyte plug. The mixtures were then electrophoretically injected into a subsequent capillary column where the faster migrating analyte bands overtook the target ligand. When the bands were co-localized, equilibrium was established (Fig. 5A) The complex signal was monitored downstream and compared with internal standard to obtain a quantitative measurement of K_d. PFACE utilized only a small section of the channel that greatly reduced the sample consumption.

aptamer and a small molecule ATP on a similar microchip architecture. However, due to the small molecular size, the mobility of the target-bound aptamer was not significantly altered, thus making it difficult to resolve the peaks. To enhance the separation, a competitor DNA molecule encoding a complementary sequence to the aptamer was added to the original reaction. The overall reaction was therefore divided into two parts: an aptamer-competitor binding and a DNA complex-ATP binding. The K_d of each was individually measured with a microfluidic EMSA. Due to the addition of competitor, the mobility shifts of the two reactions were greatly enhanced and the disassociation constant of the aptamer-ATP binding reaction was calculated as the quotient of the two K_d values.

4.2.2 Negligible disassociation: Slow dissociation rate relative to the electromigration timescale ($Da_{off} \ll 1$)

In this kinetic regime, the dissociation reaction rate is slower than electromigration. Here, bound and unbound populations remain at steady state during electrophoresis and separate from each other. As such, the dose–response relationship between the complex concentration and the target molecule is established to derive the K_d value according to Scatchard analysis.

Microfluidic EMSAs have been used to study slow-dissociating binding pairs for a wide range of applications, including fundamental molecular biology research [60, 61] and pharmaceutical drug screenings [6, 62, 63]. Clark et al. [60] studied the self-assembly performance of supramolecular protein-nucleic nanostructures on a commercially available Agilent DNA 7500 labchip. All forms of the assembly structure with different stoichiometry of the DNA backbone and associating proteins are observed, however, with much lower sample consumption benchmarking the slab gel results. Hu and Easley [61] studied the binding reaction between a DNA

4.2.3 Negligible re-association: Slow binding rate and intermediate/fast dissociation rate relative to the electromigration timescale ($Da_{on} \ll 1$ and $Da_{off} \geq 1$)

In this kinetic regime, electromigration is faster than the association timescale and slower than or equal to the dissociation timescale. During electrophoresis, continuous dissociation of the bound complex is accompanied by negligible reassociation, corresponding to a decreasing concentration of the electromigrating complex band.

Thrombin and a thrombin binding aptamer are an example of such a pair [64]. Gong et al. measured the K_d of this binding pair on a standard cross-channel microchip via fluorescence detection. The labeled aptamer was mixed with thrombin and incubated off-chip in solution followed by electrophoretic separation of the mixture. Due to disassociation, a third bridging band of the disassociated aptamer signal was observed between the free aptamer and complex on the electropherogram. To quantify the complex concentration, the area of the additional "bridge" was added back into the remaining complex band to account for the original complex

concentration before electrophoresis. The concentration ratios were then used to construct the K_d value. However, the quality of the measurement was heavily dependent on subsequent mathematical processing of the signal. No comprehensive understanding of the peak shape of the bridging signal exists. To address the problem, Cheow and Han [65] developed a new affinity assay called electrokinetic concentration affinity probe electrophoresis, which systematically accounted for complex disassociation. The authors studied the interaction between IgE/HIV transcriptor and corresponding aptamers. A core element is an ion selective Nafion membrane, which was inserted into a PDMS channel that selectively blocked the flow of anionic species (Fig. 5B). The channel was filled with buffer solution and upon electrophoresis an ion depletion zone was formed in the vicinity of the Nafion membrane due to concentration polarization. A high electric field gradient was thus formed in the ion depleted region and the advancing analytes were focused where electrophoretic and electroosmotic forces balanced. Large molecular complexes with smaller mobilities focused at regions with higher electric field strengths than smaller free aptamers, which focused at regions with lower electric field strengths. During focusing, dissociated aptamers migrated down the electric field gradient and reassociated with the continuous flow of ligand protein. These complexed species then focused at the original complex location. The "disassociation, defocusing, reassociation, refocusing" loop counteracted weak binding, achieving enhanced measurement accuracy and detection sensitivity. The negligible binding kinetics region remains one of the most challenging regimes to probe with affinity-based microfluidic EMSAs. We anticipate that the advent of new analytical tools will be needed to address the problem of molecular complex disassociation.

4.3 Microfluidic EMSAs for binding kinetics measurements

The kinetics of a binding reaction are studied by directly measuring the binding rate constants k_{on} or k_{off}. Microfluidic EMSAs developed for these kinetics measurements are divided into two categories: the first focused on obtaining k_{on} values through study of the dynamics of an association process and the second focused on deriving k_{off} from study of the disassociation process. In both cases, the time-dependent concentration change of the bound species complex is monitored for quantification.

Microfluidic EMSAs for k_{on} determination are typically effective in the slow disassociation kinetics regime. Such assays typically involve a timed incubation step for the binding reaction with subsequent quantification of the concentration of bound analyte. From such data, a kinetic curve can be constructed. Huber et al. [66] introduced nanofluidics for DNA hybridization assays and developed a free-solution platform for enhanced electrokinetic separations. The nanofluidic device was composed of two crossing channels, which were used for sample loading and separation. One end of the load-

ing channel was branched into two side channels, with terminal reservoirs for sample loading. The other side of the channel terminated in a sample waste well. The separation channel was filled with running buffer and connected the buffer well with buffer waste wells. A DNA sample and its complementary fluorescently labeled probe DNA were loaded on the nanofluidic device from the two sample loading wells, then allowed to mix/hybridize in-chip for set durations. After incubation, the sample was subjected to an electrophoretic separation. Results showed ssDNA separated from dsDNA "complex", yielding ssDNA concentration as a function of total hybridization time. The k_{on} values were calculated by fitting the data to a second-order binding reaction model. Further applications of the nanofluidic assay include binding kinetic measurements for oligonucleotides pairs with single nucleotide mismatch, thus showing the potential of such a device to the wide range of applications that would benefit from DNA hybridization.

For $Da_{on} \ll 1$ and $Da_{off} \geq 1$, measurement of k_{off} relies on monitoring the disassociation of a complex during electrophoretic analysis of an equilibrated mixture. Gong et al. [64] monitored the dissociation process between thrombin and a thrombin aptamer by measuring changes in the thrombin-aptamer complex under the curve during the separation, allowing these researchers to determine k_{off}. The initial concentration of the thrombin-aptamer complex and the migration time for the complex to traverse from the injector to the detector locations yielded k_{off}. To improve the measurement precision, Bromberg et al. [23] designed a serpentine separation channel interfaced with a rotary detector. The detector can be moved, thus allowing the system to record electropherograms at several locations along the axis of the serpentine channel. Exponential decay fit of the bound complex concentration yields an accurate k_{off} value for TNT and its antibody.

Importantly, measurement of k_{off} using microfluidic EMSAs is feasible for a subset of binding kinetics regimes. To be effective at assessing k_{off}, the timescales of the electrophoretic separation and of the molecular binding must be similar. On the one hand, if the separation proceeds too quickly as compared to dissociation, loss of complex will not be observed. On the other hand, if the separation is too slow as compared to the dissociation, only unbound (free) species will be observed. Switching to a heterogeneous assay may allow an observer to monitor the disassociation process in regimes inaccessible to homogeneous EMSAs.

4.4 Other size/charge-based microfluidic EMSAs

4.4.1 Drag-tag-based microfluidic EMSAs

Another major class of microfluidic electrophoresis assays uses molecular "drag-tags" to induce a detectable and controllable molecular mass change and, hence, an electrophoretic mobility shift for the target analyte. Molecular tagging has been typically accomplished through chemical conjugation

or electrostatic attraction. A drag-tag-induced mobility shift has been shown to improve the separation resolution, especially for samples that are otherwise difficult to fractionate. The Barron group developed microfluidic "drag-tag" electrophoretic tools for a series of applications including detection of SNPs [67], detection of point mutations with ligase detection reaction [68,69], determination of the primer-dimer formation risk [70], and DNA size-based separations [71] in free solution. For the primer-dimer formation [70], the "drag-tag" is used to enhance the separation resolution in the free solution between the single-stranded primer and the double-stranded dimer that are of identical mass/charge ratio. To resolve the two populations, a chemically synthesized poly-*N*-methoxyethylglycine drag-tag was attached to one primer in the dimer to induce a mobility shift from the free form primer, allowing quantification of hybridization. Using the approach, primers with different complementary lengths have been investigated (i.e. binding affinity, melting point). In a DNA sizing assay [71], a positively charged protein polymer was conjugated to the target oligonucleotide and subsequent free-solution electrophoretic separation reported molecular size. The protein-based drag-tag significantly changed the size-to-charge ratio, amplifying the mobility difference between oligonucleotides with only a few base pair differences. As may be hypothesized, the larger the protein polymers, the better the fractionation performed. The drag-tags eliminated the need for a molecular sieving matrix and DNA molecules up to 400 base pairs (bp) in length were sequenced with a resolution of 2 bp. With the DNA sizing assay, Albrecht et al. [69] successfully screened 19 K-ras oncogene mutation ligase detection reaction products ranging in size from 42 to 66 nt simultaneously in one run. Further development as a sieving matrix-free DNA sequencing assay on a microchip is likely to follow, given the previously successful sequencing of up to 180 bp in CE [72].

4.4.2 Microfluidic EMSAs as specific enantiomer selectors

Microfluidic EMSAs have been adapted into affinity-based selectors for specific enantiomers. Weng et al. [9] developed a microfluidic chip housing separation channels with surfaces modified by BSA-conjugated single-wall carbon nanotubes (SWNTs). The device was introduced to separate tryptophan enantiomers. The SWNTs acted as a monolithic stationary phase, being chemically attached to the wall of a PMMA microchannel. BSA, which has different binding affinities to DL-tryptophan, was conjugated to the body of SWNT to select for specific chiral forms during electrophoresis. In designing a microfluidic EMSA chiral selector assay, the amount of affinity probe immobilized on the channel wall determines separation quality, making the choice of stationary phase material essential to the success of the assay. Li et al. [73] employed gold-nanoparticle BSA as a stationary phase and separated a mixture of ephedrine and norephedrine isomers. On top of

that, a later study [74] showed thiolated β-CD-modified gold nanoparticles allowed for easier fabrication and improved microchip stability. Other microfluidic enantiomer selection studies are reviewed in [75].

5 Critical challenges and future trends

5.1 Innovation in microfluidic EMSA platforms for binding affinity measurements

Microfluidic EMSAs possess strong quantitative analytical capabilities and have been utilized in a wide range of applications including conformational change analysis, IAs, electrophoretic affinity assays, and DNA sizing/sequencing assays. The miniaturized format and resolving power enables detection of small mobility shifts that are not resolvable on standard macroscale slab-gel EMSAs or capillary formats. Efforts are ongoing in the following areas:

(i) Innovative affinity EMSAs designed for K_d measurement across a wide range of kinetic regions. Homogeneous microfluidic EMSA affinity assays have difficulty in characterizing binding pairs having "negligible re-association" kinetics. As pointed out earlier, continuous disassociation of molecular complexes during electrophoresis prevents precise quantification of the respective analyte concentrations (bound, free). A few microfluidic platforms have been proposed that may potentially tackle this problem [64, 65]. Nevertheless, conventional CE based affinity assays have successfully addressed the problem through separation modes including the Hummel–Dreyer method [76], vacancy ACE [77], and the vacancy-peak method [78], which have not yet been adapted to a microfluidic device. Consequently, future efforts may focus on adopting these approaches on a microfluidic EMSA format to broaden the analytical capability.

(ii) Heterogeneous microfluidic electrophoresis platforms to study kinetic rate constants of binding pairs across a wide range of kinetic regimes. As pointed out earlier, the mismatch between the electromigration rate and the binding kinetics in homogeneous EMSAs limits k_{off} analyses. Limitations are particularly acute in regimes with negligible reassociation. Further introduction of heterogeneous formats for EMSA-like performance may improve analytical access to this space. In such formats, the affinity probe is immobilized and continuously reacts with migrating analytes, allowing dynamic recording of the entire kinetic process. One approach utilizes functional hydrogels patterned inside microchannels, which, for example, has been demonstrated for microfluidic PLE [44,79]. Photopatterning of capture partners may prove useful, especially regarding multiplexing in simple channel geometries [80].

5.2 Additional applications for microfluidic EMSAs

Microfluidic EMSAs rely on affinity-based probing of a target analyte, yet the approach is not necessarily limited to IAs and affinity measurements. As detailed in Sections 4.3 and 4.4, microfluidic EMSAs are widely exploited for DNA sizing, genomic sequencing, point mutation detection, and chiral separations. In the future, microfluidic EMSAs may see expanded use as screening/selection assays compatible with large libraries of target molecules. For example, capillary electrophoresis-systematic evolution of ligands by exponential enrichment (CE-SELEX) has been studied by Mendonsa and Bowser [81] with a distinguishable mobility shift in a target-bound aptamer. CE-SELEX allows rapid selection of target molecules, with high partitioning efficiency and a lower number of processing cycles as compared to traditional SELEX. We imagine future efforts in miniaturization of CE-SELEX with more efficient target selection and post-EMSA sample collection. In addition, microfluidic EMSAs may advance drug discovery by the pharmaceutical industry. Large amounts of drug candidate molecules can be screened in a few minutes on the high-throughput microfluidic EMSA platform [6, 62], potentially bringing a tremendous reduction to cost of drug development [82].

The authors have declared no conflict of interest.

6 References

[1] Harrison, D. J., Manz, A., Fan, Z. H., Ludi, H., Widmer, H. M., *Anal. Chem.* 1992, *64*, 1926–1932.

[2] Herr, A. E., Singh, A. K., *Anal. Chem.* 2004, *76*, 4727–4733.

[3] Garcia-Schwarz, G., Santiago, J. G., *Anal. Chem.* 2012, *84*, 6366–6369.

[4] Grunwald, M. E., Yu, W. P., Yu, H. H., Yau, K. W., *J. Biol. Chem.* 1998, *273*, 9148–9157.

[5] Park, S.-H., Raines, R., in: Fu, H. (Ed.), *Methods Mol. Biol.* 2004, *261*, 155–160.

[6] Perrin, D., Fremaux, C., Besson, D., Sauer, W. H. B., Scheer, A., *J. Biomol. Screen* 2006, *11*, 996–1004.

[7] Karns, K., Vogan, J. M., Qin, Q., Hickey, S. F., Wilson, S. C., Hammond, M. C., Herr, A. E., *J. Am. Chem. Soc.* 2013, *135*, 3136–3143.

[8] Apori, A. A., Herr, A. E., *Anal. Chem.* 2011, *83*, 2691–2698.

[9] Weng, X. X., Bi, H. Y., Liu, B. H., Kong, J. L., *Electrophoresis* 2006, *27*, 3129–3135.

[10] Chu, Y. H., Avila, L. Z., Biebuyck, H. A., Whitesides, G. M., *J. Med. Chem.* 1992, *35*, 2915–2917.

[11] Liu, X. J., Dahdouh, F., Salgado, M., Gomez, F. A., *J. Pharm. Sci.* 2009, *98*, 394–410.

[12] Hou, C., Herr, A. E., *Electrophoresis* 2008, *29*, 3306–3319.

[13] Shanmuganathan, M., Britz-McKibbin, P., *Anal. Chim. Acta* 2013, *773*, 24–36.

[14] Jiang, C. X., Armstrong, D. W., *Electrophoresis* 2010, *31*, 17–27.

[15] Rundlett, K. L., Armstrong, D. W., *Electrophoresis* 2001, *22*, 1419–1427.

[16] Reccius, C. H., Stavis, S. M., Mannion, J. T., Walker, L. P., Craighead, H. G., *Biophys. J.* 2008, *95*, 273–286.

[17] Cross, J. D., Strychalski, E. A., Craighead, H. G., *J. Appl. Phys.* 2007, *102*, 024701-024701-5.

[18] Sacca, B., Niemeyer, C. M., *Angew. Chem. Int. Edit.* 2012, *51*, 58–66.

[19] Park, H. Y., Kim, S. A., Korlach, J., Rhoades, E., Kwok, L. W., Zipfell, W. R., Waxham, M. N., Webb, W. W., Pollack, L., *Proc. Natl. Acad. Sci. USA* 2008, *105*, 542–547.

[20] Chiem, N. H., Harrison, D. J., *Electrophoresis* 1998, *19*, 3040–3044.

[21] Qiu, C. X., Harrison, D. J., *Electrophoresis* 2001, *22*, 3949–3958.

[22] Cheng, S. B., Skinner, C. D., Taylor, J., Attiya, S., Lee, W. E., Picelli, G., Harrison, D. J., *Anal. Chem.* 2001, *73*, 1472–1479.

[23] Bromberg, A., Mathies, R. A., *Anal. Chem.* 2003, *75*, 1188–1195.

[24] Bromberg, A., Mathies, R. A., *Electrophoresis* 2004, *25*, 1895–1900.

[25] Huang, Y., Shi, M., Zhao, S. L., Liang, H., *Electrophoresis* 2011, *32*, 3196–3200.

[26] Huang, Y., Zhao, S. L., Shi, M., Liu, Y. M., *Anal. Biochem.* 2010, *399*, 72–77.

[27] Huang, Y., Zhao, S. L., Shi, M., Liu, J. W., Liang, H., *Anal. Chim. Acta* 2011, *694*, 162–166.

[28] Huang, Y., Zhao, S. L., Shi, M., Liu, J. W., Liang, H., *Electrophoresis* 2012, *33*, 1198–1204.

[29] Zhao, S., Liu, Y. M., *Methods Mol. Biol.* 2013, *919*, 79–85.

[30] Shackman, J. G., Dahlgren, G. M., Peters, J. L., Kennedy, R. T., *Lab Chip* 2005, *5*, 56–63.

[31] Reid, K. R., Kennedy, R. T., *Anal. Chem.* 2009, *81*, 6837–6842.

[32] Dishinger, J. F., Kennedy, R. T., *Anal. Chem.* 2007, *79*, 947–954.

[33] Dishinger, J. F., Reid, K. R., Kennedy, R. T., *Anal. Chem.* 2009, *81*, 3119–3127.

[34] Schmalzing, D., Koutny, L. B., Taylor, T. A., Nashabeh, W., Fuchs, M., *J. Chromatogr. B* 1997, *697*, 175–180.

[35] Phillips, T. M., *Electrophoresis* 2004, *25*, 1652–1659.

[36] Phillips, T. M., Wellner, E., *J. Chromatogr. A* 2006, *1111*, 106–111.

[37] Phillips, T. M., Wellner, E. F., *Electrophoresis* 2007, *28*, 3041–3048.

[38] Herr, A. E., Hatch, A. V., Throckmorton, D. J., Tran, H. M., Brennan, J. S., Giannobile, W. V., Singh, A. K., *Proc. Natl. Acad. Sci.* 2007, *104*, 5268–5273.

[39] Karns, K., Herr, A. E., *Anal. Chem.* 2011, *83*, 8115–8122.

[40] Hou, C. L., Herr, A. E., *Anal. Chem.* 2010, *82*, 3343–3351.

[41] Margolis, J., Kenrick, K. G., *Nature* 1967, *214*, 1334–1336.

[42] Lo, C. T., Throckmorton, D. J., Singh, A. K., Herr, A. E., *Lab Chip* 2008, *8*, 1273–1279.

[43] Ng, A. H. C., Uddayasankar, U., Wheeler, A. R., *Anal. Bioanal. Chem.* 2010, *397*, 991–1007.

[44] Chen, X., Kapil, M. A., Hughes, A. J., Herr, A. E., *Anal. Chem.* 2011, *83*, 6573–6579.

[45] Sommer, G. J., Singh, A. K., Hatch, A. V., *Lab Chip* 2009, *9*, 2729–2737.

[46] Gao, Y. L., Shermanb, P. M., Sun, Y., Li, D., *Anal. Chim. Acta* 2008, *606*, 98–107.

[47] Hu, G. Q., Gao, Y. L., Sherman, P. M., Li, D. Q., *Microfluid. Nanofluid.* 2005, *1*, 346–355.

[48] Hu, G., Gao, Y., Li, D., *Biosens. Bioelectron.* 2007, *22*, 1403–1409.

[49] Araz, M. K., Akwasi, A. A., Salisbury, C. M., Herr, A. E., *Lab Chip* 2013, *13*, 3910–3920.

[50] Pan, Q., Hong, S., Zhu, X. C., Zhao, M. P., Lee, L. P., *Lab Chip* 2012, *12*, 932–938.

[51] Kagebayashi, C., Yamaguchi, I., Akinaga, A., Kitano, H., Yokoyama, K., Satomura, M., Kurosawa, T., Watanabe, M., Kawabata, T., Chang, W., Li, C., Bousse, L., Wada, H. G., Satomura, S., *Anal. Biochem.* 2009, *388*, 306–311.

[52] Park, C. C., Kazakova, I., Kawabata, T., Spaid, M., Chien, R. L., Wada, H. G., Satomura, S., *Anal. Chem.* 2008, *80*, 808–814.

[53] Kawabata, T., Wada, H. G., Watanabe, M., Satomura, S., *Electrophoresis* 2008, *29*, 1399–1406.

[54] Mohamadi, M. R., Kaji, N., Tokeshi, M., Baba, Y., *Anal. Chem.* 2007, *79*, 3667–3672.

[55] Cann, J. R., *Anal. Biochem.* 1996, *237*, 1–16.

[56] Chuang, Y. J., Huang, J. W., Makamba, H., Tsai, M. L., Li, C. W., Chen, S. H., *Electrophoresis* 2006, *27*, 4158–4165.

[57] Stettler, A. R., Schwarz, M. A., *J. Chromatogr. A* 2005, *1063*, 217–225.

[58] Stettler, A. R., Krattiger, P., Wennemers, H., Schwarz, M. A., *Electrophoresis* 2007, *28*, 1832–1838.

[59] Brown, A., Morales, C., Gomez, F. A., *Talanta* 2008, *74*, 605–612.

[60] Clark, J., Shevchuk, T., Swiderski, P. M., Dabur, R., Crocitto, L. E., Buryanov, Y. I., Smith, S. S., *Biotechniques* 2003, *35*, 548–554.

[61] Hu, J. M., Easley, C. J., *Analyst* 2011, *136*, 3461–3468.

[62] Perrin, D., Fremaux, C., Scheer, A., *J. Biomol. Screen.* 2006, *11*, 359–368.

[63] Fanslau, C., Pedicord, D., Nagulapalli, S., Gray, H., Pang, S. H., Jayaraman, L., Lippy, J., Blat, Y., *Anal. Biochem.* 2010, *402*, 65–68.

[64] Gong, M., Nikcevic, I., Wehmeyer, K. R., Limbach, P. A., Heineman, W. R., *Electrophoresis* 2008, *29*, 1415–1422.

[65] Cheow, L. F., Han, J. Y., *Anal. Chem.* 2011, *83*, 7086–7093.

[66] Huber, D. E., Markel, M. L., Pennathur, S., Patel, K. D., *Lab Chip* 2009, *9*, 2933–2940.

[67] Meagher, R. J., Coyne, J. A., Hestekin, C. N., Chiesl, T. N., Haynes, R. D., Won, J. I., Barron, A. E., *Anal. Chem.* 2007, *79*, 1848–1854.

[68] Sinville, R., Coyne, J., Meayher, R. J., Cheng, Y. W., Barany, F., Barron, A., Soper, S. A., *Electrophoresis* 2008, *29*, 4751–4760.

[69] Albrecht, J. C., Kotani, A., Lin, J. S., Soper, S. A., Barron, A. E., *Electrophoresis* 2013, *34*, 590–597.

[70] Desmarais, S. M., Leitner, T., Barron, A. E., *Electrophoresis* 2012, *33*, 483–491.

[71] Albrecht, J. C., Kerby, M. B., Niedringhaus, T. P., Lin, J. S., Wang, X. X., Barron, A. E., *Electrophoresis* 2011, *32*, 1201–1208.

[72] Meagher, R. J., Won, J. I., Coyne, J. A., Lin, J., Barron, A. E., *Anal. Chem.* 2008, *80*, 2842–2848.

[73] Li, H. F., Zeng, H. L., Chen, Z. F., Lin, J. M., *Electrophoresis* 2009, *30*, 1022–1029.

[74] Li, M., Liu, X., Jiang, F. Y., Guo, L. P., Yang, L., *J. Chromatogr. A* 2011, *1218*, 3725–3729.

[75] Nagl, S., Schulze, P., Ludwig, M., Belder, D., *Electrophoresis* 2009, *30*, 2765–2772.

[76] Kraak, J. C., Busch, S., Poppe, H., *J. Chromatogr.* 1992, *608*, 257–264.

[77] Busch, M. H. A., Boelens, H. F. M., Kraak, J. C., Poppe, H., *J. Chromatogr. A* 1997, *775*, 313–326.

[78] Vlckova, M., Stettler, A. R., Schwarz, M. A., *J. Liq. Chromatogr. Relat. Technol.* 2006, *29*, 1047–1076.

[79] Hughes, A. J., Herr, A. E., *Anal. Chem.* 2010, *82*, 3803–3811.

[80] Hughes, A. J., Lin, R. K. C., Peehl, D. M., Herr, A. E., *Proc. Natl. Acad. Sci. USA* 2012, *109*, 5972–5977.

[81] Mendonsa, S. D., Bowser, M. T., *J. Am. Chem. Soc.* 2004, *126*, 20–21.

[82] Karns, K., Herr, A. E., *Bioanalysis* 2011, *3*, 2161–2165.